Organic & Biomolecular Chemistry

PAPER

View Article Online
View Journal | View Issue

Cite this: *Org. Biomol. Chem.*, 2017, **15**, 7936

A fluorescent pH probe for acidic organelles in living cells†

Jyun-Wei Chen,[a] Chih-Ming Chen*[a] and Cheng-Chung Chang *[b]

Received 16th August 2017,
Accepted 4th September 2017

DOI: 10.1039/c7ob02037f

rsc.li/obc

A water-soluble pH sensor, 2-(6-(4-aminostyryl)-1,3-dioxo-1*H*-benzo[*de*]isoquinolin-2(3*H*)-yl)-*N*,*N*-dimethylethanamine (ADA), was synthesized based on the molecular design of photoinduced electron transfer (PET) and intramolecular charge transfer (ICT). The fluorescence emission response against a pH value is in the range 3–6, which is suitable for labelling intracellular pH-dependent microenvironments. After biological evolution, ADA is more than a pH biosensor because it is also an endocytosis pathway tracking biosensor that labels endosomes, late endosomes, and lysosome pH gradients. From this, the emissive aggregates of ADA and protonated-ADA in these organs were evaluated to explore how this probe stresses emission colour change to cause these unique cellular images.

Introduction

Acid–base (pH) balance is a key parameter for cell survival.[1] For example, a higher intracellular pH (≥7.4) and a lower extracellular pH (~6.7–7.1) exist in cancer cells compared with normal cells (intracellular pH ~ 7.2; extracellular pH ~ 7.4) to form a 'reversed' pH gradient[2] that promotes proliferation, cancer cell invasion, and escape from apoptosis.[3] Moreover, acid–base dysregulation is a common property of cancer cells that may affect the uptake and efficacy of pH-sensitive chemotherapeutic drugs.[4] Thus, the differences in pH between normal and cancer cells may provide a diagnostic tool by using a pH probe. In addition, tracing pH fluctuations in acidic organelles is essential to investigate normal cellular functions and activities in these compartments.

The endocytosis pathway is a process by which cells internalize biomolecules that are associated with numerous biological processes.[5] In these pathways, every attended organelle maintains a unique pH value to provide the appropriate biochemical conditions. The pH gradient follows the endocytic pathway as ~6.3 in early endosomes, ~5.5 in late endosomes, and ~4.6 in lysosomes. The apparent decline of proton flow in the endocytosis pathway provides a good switch for a fluorescence biosensor.[6] The strategy for measuring the intracellular pH gradient is based on the design of the fluorophore, which could reveal emission response, colour or intensity with the association or dissociation of protons. This is because fluorescence detection allows non-invasive measurements with biological objects, parallel monitoring of multiple samples, and imaging.[7] Therefore, ratiometric fluorescence measurement is more desired.[8] However, most pH fluorescent probes lack sensitivity or are not suitable for characterizing acidic organelles such as lysosomes, endosomes, and spermatozoa acrosomes, because their emissions are weak or disappear in concentrated solutions or in acidic environments due to aggregation-caused fluorescence quenching or changes in intramolecular charge transfer (ICT). This is inevitable because the molecules or probes become encapsulated inside endocytic vesicles through clustering in the endocytosis pathway. Under these conditions, a fluorophore which is highly fluorescent in the concentrated state, would be a good choice to overcome this challenge by tracing endocytic or lysosome vehicles.

Based on our knowledge, the aggregation induced emission (AIE),[9] aggregation induced emission enhancement (AIEE)[10] and non-resonant exciton system[11] are widely used to explain the aggregation-dependent fluorescence enhancement behaviours of molecules. The so-called AIE/AIEE dyes are characterized by their enhanced emission, usually from non-emissive molecular states in organic solutions to strongly emitting aggregate states in aqueous media, mostly due to conformational restriction[9,10,12] or planarization of "non-flat" molecules.[13] Aggregation-dependent non-fluorescence or fluorescence enhancement behaviours of "flat" aromatic dyes should be discussed in the context of a non-resonant exciton system because there are no conformational restriction problems in these planar molecules. These flat molecules can form intermolecular stacks with each other in the concen-

[a]*Department of Chemical Engineering, National Chung Hsing University, Taichung 402, Taiwan*
[b]*Graduate Institute of Biomedical Engineering, National Chung Hsing University, Taichung 402, Taiwan. E-mail: ccchang555@dragon.nchu.edu.tw*

† Electronic supplementary information (ESI) available: Synthesis and characterisation, Fig. S1–S8, Table S1. See DOI: 10.1039/c7ob02037f

trated or solid state and lead to an emissive non-resonance excitonic state of H-aggregates or emissive J-aggregates.[11,14] We proposed that these aggregation caused emission molecules, as mentioned above, should brighten the defect and protonation induced fluorescence quenching once they are encapsulated by endosomes and become vehicles in the endocytosis pathways. In addition, there is a serious need for the development of multicolour fluorogens for pH detection, which usually correlates to discussions about J-aggregate formation, *E*/*Z* isomerization, twisted intramolecular charge transfer (TICT), and excited state intramolecular proton transfer (ESIPT).[15,16]

In the present study, a pH-response fluorophore, ADA, was designed and synthesized by incorporating a dimethylaminoethylamine group, a proton acceptor, into 1,8-naphthalic anhydride to become a naphthalimide core scaffold, which further elongated the π-electronic resonance by conjugating a vinyl aniline functional group. The water-soluble fluorophore ADA presents red to green emissions when exposed to relatively neutral to acidic conditions. Its pH dependent AIE behaviour was also investigated to help explain intracellular molecular imaging, which was further investigated in live intracellular images, time-dependent imaging, concentration-dependent images, and subcellular localization. Finally, we observed that intracellular luminous behaviour for ADA molecules was dependent on pH values in the endocytosis pathway and could be applied to the distinct intracellular pH gradient of the endocytosis pathway.

Results and discussion

Molecular design and synthesis

Naphthalimide is a good electron acceptor to be used to design spectral pH-response compounds.[17] In this study, the D–π-A type chromophore structure was designed and synthesized by incorporating an electron donor group to naphthalimide by means of the π-conjugated linker ethylene. At first, the starting material, 4-bromo-1,8-naphthalic anhydride, was initially reacted with *N*,*N*-dimethyl-ethylenediamine (for NIM-1/ADA) or *n*-butylamine (for ANB) to form the naphthalimide core scaffold. Then, the 4-vinylamine (for ANB/ADA) and 4-methoxyphenyl (for NM-1) functional groups, or electron-donating units, were chosen to substitute the 4-positions of naphthalimide by Heck organic–metal coupling reactions. In Fig. 1a, the pH-responsive fluorophore ADA is constructed by introducing a tertiary amine substituent ($pK_a \sim 10$ of conjugate acidic species) and vinylaniline ($pK_a \sim 4.73$) as a protonation site to increase water solubility with the expectation that ADA will accumulate in acidic organelles in its protonated form.[18] Furthermore, the electron donor dimethylamine acts as a PET quencher and aniline acts as an ICT responsive moiety related to naphthalene. Hence, the control compounds NIM-1 and ANB were prepared according to the relative optical properties. Compared with these control compounds, we could easily understand the two-stage acidification process of ADA.

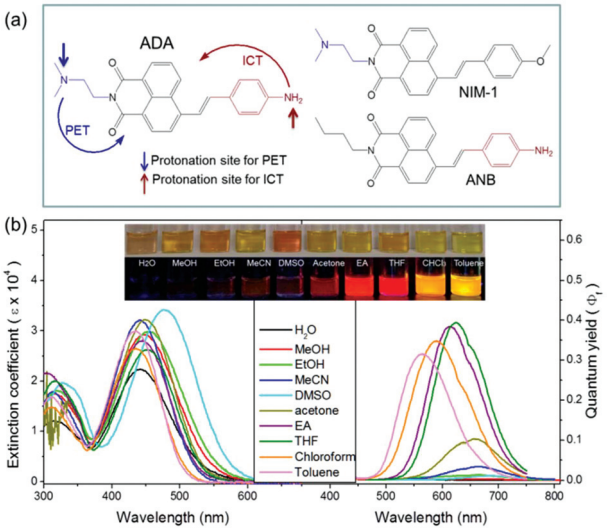

Fig. 1 (a) Chemical structure and push–pull illustration of the compounds ADA, NIM-1 and ANB. Arrows indicate the protonation site. (b) Solvent effect of compound ADA under neutral conditions, represented by the extinction coefficient for absorbance and quantum yield for emission spectra.

Particular optical properties

Fig. 1b presents broad absorption peaks with a slight solvent effect, and low quantum yield emission peaks were observed in high-polarity solvents; brighter emissions with high quantum yields were obtained in lower polarity solvents. Compared to the solvent effects of the control compounds NIM-1 and ANB (Fig. S1†), the basic spectral properties of ADA are similar to ANB but not NIM-1 with lower quantum yields. Its absorption spectra showed two main peaks at 310 to 330 nm, assigned to the π–π* transition, and at 435 nm (in toluene) to 477 nm (in DMSO), which was assigned to the internal charge transfer (ICT) characteristic of the fluorophore with the push–pull effect between the electron donating aniline and the electron withdrawing naphthalimide.[19]

The spectra of ADA were first investigated as a function of pH in water. Fig. 2a shows that upon titration with an acid, the 440 nm peak shifted hypsochromically to 395 nm with an isosbestic point at 415 nm. Meanwhile, upon excitation of the ICT band at 440 nm, a peak appears with λ_{em} max at 515 nm, which becomes more apparent once excitation was 395 nm, *i.e.*, the absorption of protonated ADA. This observed emission change is highly pH dependent and is 'switched on' upon acidification with large fluorescence enhancements. The plot of absorbance at 440 nm against pH showed only minor changes that occurred above pH 6.2, while the most significant changes were observed between pH 3 and 6. From this dynamic region, a $pK_a \sim 5.07$ was determined using non-linear regression analysis. Similar pK_a values were also determined by plotting the emission at 515 nm against pH, and the pK_a value at ~3.64 was unclearly found. The pH-dependent spectral change under aqueous conditions was not apparent enough to estimate two pK_a values for ADA.

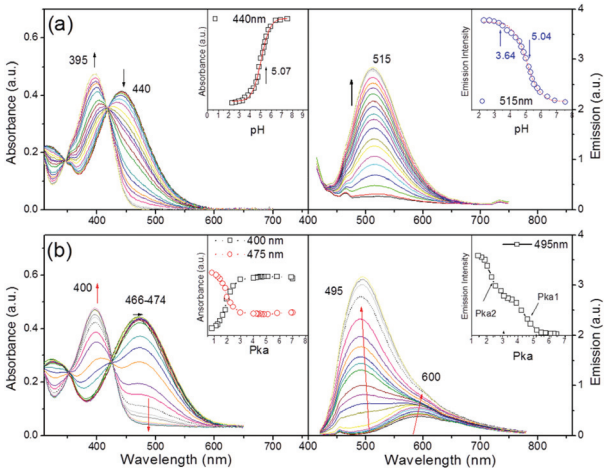

Fig. 2 ADA (30 μM) absorption (left) and emission (right) spectral variations as a function of addition of [H^+] in (a) dd-water and (b) DMSO/H_2O = 3/1 in v/v. Inserts show peak intensity plots against pH (excited wavelength = 400 nm).

Hence, we investigated the spectral variations of ADA protonation in DMSO/H_2O solutions with 0, 1/3, and 1/2 H_2O in volume proportion. Preparations of pH-dependent DMSO/H_3O^+ solutions are described in the Experimental section. Fig. 2b shows the spectral changes as a function of pH for ADA compounds in DMSO/H_2O (3/1, v/v). When the environment was changed from neutral to acidic, the λ_{abs} was first redshifted from 466 to 474 nm and then began to decrease. At the same time, a new absorption peak at ~400 nm grew with a 423 nm isosbestic point. Once we fixed the excited wavelength at 400 nm to track the titration emission spectra, there were two emission peaks at ~600 and 495 nm that grew simultaneously with different increasing rates. This phenomenon becomes more obvious on increasing the amount of DMSO, and the two-step protonation behaviour becomes clearer, as shown in Fig. 2a, b and Fig. S2.† On the other hand, in Fig. S3 and S4† we checked the pH-titration spectra of the control compounds NIM-1 and ANB before the characterization of the possible protonated forms of ADA. At the beginning of the titration process, a spectral variation of ADA was similar to NIM-1. Absorption and emission spectra showed only minor changes with pH variations but were slightly redshifted. For ideal PET sensors, such shifts do not usually occur. We believe that this is due to the protonation inhibition of PET from dimethylamine to naphthalene. This further affects the ICT between naphthalene and anisole (or aniline). In contrast, ANB showed apparent changes in its absorption and emission spectra as a function of pH in DMSO, which is similar to the spectral change against pH, as ADA showed at a later period of titration. The marked red-to-green emission colour change in response to the change in pH should be the cause of protonation of the aniline moiety inducing a push–pull decrease as well as an ICT change.[20]

The pK_{a1} value (5.04 from aqueous and 4.81 from DMSO/H_2O) corresponds to the protonated form of dimethylamine, which is likely due to the PET decrease between dimethylamine and an electron donating group-substituted naphthalene at the 4-position. Meanwhile the pK_{a2} value (3.64 from aqueous and 2.68 from DMSO/H_2O) corresponds to the protonated form of the aniline moiety of ADA, which is because the electron donation ability of the NH_2 long pair was shared with naphthalene *via* a vinyl group. Moreover, when we checked the viscosity-variation response emission spectra in Fig. S5,† both emission peaks (~600 nm and ~500 nm) presented positive ICT responses to a high-viscosity environment. From the discussion above, the emission peak at ~600 nm was characterized as a PET induced ICT change of ADA-H, and the emission peak at ~500 nm indicated the ICT change of ADA-H_2. Eventually, the pH response emission changes of ADA cover dimethylamine, aniline (~4.87, 4.6), 4-vinyl aniline (~4.73), and the fluorescent pH indicator Oregon Green® 488 (~4.7),[21] which demonstrates that this compound is suitable for the physiological pH range.

pH-Dependent fluorescence mapping

MRC-5 human lung fibroblast normal cell lines, HeLa human cervix epithelial adenocarcinoma cells and CL1-0 human lung adenocarcinoma cells were selected for cellular imaging studies. Fig. 3 shows the cellular imaging of these cell lines treated with ADA for four hours and then observed by fluorescence microscopy with a colour CCD to obtain the real emission colour of intracellular ADA. It is interesting that colourful bright spots were revealed in all three cell lines and that MRC-5 normal cells exhibited the most abundant fluorescent colours (Fig. 3b and c). When checking the intracellular molecular imaging of the control compound NIM-1, Fig. S6† shows similar bright spots, but no apparent fluorescent colour change as well as fewer bright spots with a unitary fluorescent colour appeared in the ANB case. It appears that ADA showed

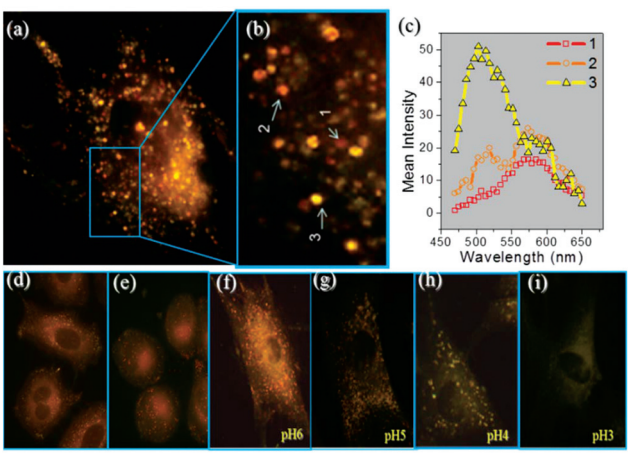

Fig. 3 Fluorescence images of (a) MRC-5 normal, (d) HeLa and (e) CL1-0 cancer cells stained with ADA (5 μM) for 4 hours; (b) magnified version of (a); (c) confocal λ scanning, 470 to 650 nm with 5 nm integration, of (b). (f)–(i) Several selected images from the MRC-5 cells pre-loaded with 5 μM ADA were incubated with nigericin and subsequently imaged in pH ~ 6, 5, 4 and 3 buffers (cube: ex, 390/10 nm; em, 410 nm lp filter).

special cellular images that combine the intracellular molecular imaging of the control compounds NIM-1 and ANB. Moreover, these colourful fluorescence spots varied and showed a different presentation between cancer and normal cells. These phenomena should be explored based on the acidic fluorescence-response image consideration. Fig. 3f–i present the pH dependent cellular imaging of ADA by addition of a H^+/K^+ exchanger ionophore nigericin.[22] Once the intracellular pH was homogenized by the surrounding medium clamped at pH 6, 5, 4 or 3, the intracellular pH gradient disappeared, and these colourful fluorescent spots become unified or faded. Hence, this proves that ADA performed fluorescence cellular imaging against the intracellular pH gradient. The change in the ratio of red to green emission intensity showed the ability of ADA to measure a pH dependent cellular signal over the pH range from 3 to 7. We interpreted ADA to be suitable for mapping the organelles relevant to the endocytosis pathway.

Subcellular localization of ADA

The endocytic pathway is composed of dynamic membrane processes in an increasingly acidic environment once the substances pass through the pathway. Endocytic vesicles are acidic, and the lysosomes can reach pH values of 4.5–4.7.[1] To determine the subcellular localization of ADA, cells were incubated with the compound ADA and then double-stained with red cellular lysosomal trackers (LysoTracker Red DND-99) and endosomal trackers (rhodamine DHPE). The rhodamine DHPE probe can be used to label biological membranes and to probe phospholipids within membranes, including pathways for endocytosis.[23] Fig. S7† shows that the bright spots of intracellular ADA can partially co-localize with lysosomal markers (co-localization was analysed by Pearson correlation coefficient (PCC): 48.2%) and rhodamine DHPE ((PCC): 65.7%). These results indicated that ADA molecules first pass through cellular membranes *via* endocytic vehicles and then accumulate in lysosomes, resulting in colourful fluorescent spots due to pH gradient values of the environments that seem to match the emission variations of the gradually protonated ADA. In the endocytosis pathway, the participating organelles maintain unique intravesicular pH values to provide an appropriate microenvironment for specific biochemical processes. Along the endocytic pathway, pH values lowered from ~6.3 in early endosomes to ~5.5 in late endosomes, then further down to ~4.6 in lysosomes.[1] Therefore, it is possible that neutral ADA can pass through the cell membrane and be protonated gradually in endosomes to reveal orange coloured fluorescent spots (green < red in Fig. 2b) during the early incubation period. Then, further protonation occurred in lysosomes and yellow spots (green > red in Fig. 2b) were observed.

Thus, to characterize the endocytic pathway-related colourful bright spots, we carefully assessed the time-dependent intracellular molecular fluorescence images (Fig. 4a). At an initial ADA incubation period between 30 minutes and 1 hour, the colourful fluorescence spots revealed abundant dark-red spots, fewer orange spots, and rare bright yellow spots. We

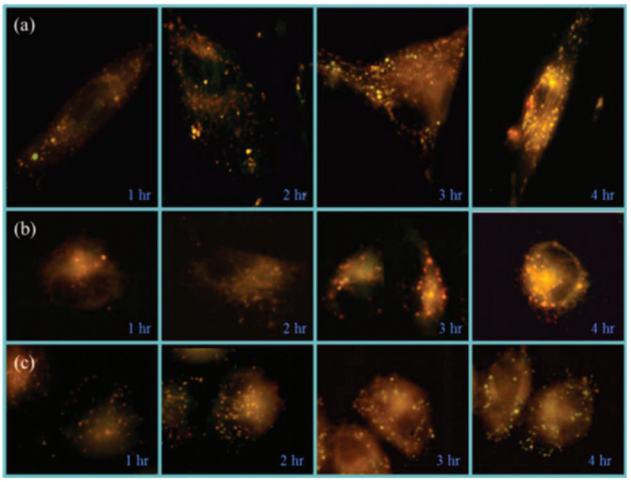

Fig. 4 A time-dependent intracellular accumulation illustration of 5 μM ADA in (a) MRC-5 normal cells, (b) HeLa cancer cells and (c) CL1-0 cancer cells. The UV cube (ex 390/10 nm, 410 long pass filter) was used to collect the images.

propose that the dark-red spots are the fluorescent presentation of a nearly neutral form of ADA in early endosomes, in which the environmental acidity is too low to protonate ADA. The orange fluorescence spots would be the late endosomes. With prolonged incubation times, these brightly coloured spots will be redistributed; the dark-red spots will disappear, and the yellow spots will become dominant, indicating lysosomes. Similar fluorescence spot-colour development was also observed in the HeLa and CL1-0 cancer cell lines, although there were fewer spot presentations (Fig. 4b and c). However, the time-dependent cellular images of NIM-1 and ANB showed no differences between incubation periods (Fig. S8 and S9†). The former could not present pH-dependent fluorescence colour changes, while the latter did not display endosomes because of its lower pK_a. That is, compound ADA provides a full range of colours for the pH scale. These results show that time-dependent images were associated with the cellular endocytosis pathway.

Formation of intracellular luminescent spots

Reviewing the optical spectral properties of ADA, we must claim that ADA in most polar solvents showed low fluorescent emission. Hence, the fluorescent brightness of intracellular molecular imaging (spots) is above what we expected. Through these phenomena, it can be proposed that the compound may remain in a nonpolar environment within the endosome. However, we observed that the quantum yields of ADA were dramatically reduced in these low polarity solvents during protonation (EA, THF, toluene *etc.*) (Table S1†). Hence, we tried to propose the involvement of other possible mechanisms to explain the intracellular bright spots, and the potential of the emissive aggregates of compound ADA was evaluated. In previous studies, we applied AIE properties to describe the fluorescence behaviour of the solid state and water-soluble fluoro-

gen and observed the formation of fluorescence organic nanoparticles (FONs).[24,25] A typical experimental demonstration is to show turn-on type fluorescence of a dye as the water content increases to a certain level where aggregates form.[26] Here, we first explored the emission spectral variations of ADA in a variable ratio of THF/H_2O or THF/(H_3O^+) mixing solutions, and we found no emission enhancement greater than that in THF (Fig. S9†). However, it is interesting that red coloured fluorescent spots (FONs) were observed under fluorescence microscopy by evaporating in a vacuum from 50 μM ADA/THF solution as shown in Fig. 5a. The TEM image was prepared from the same solution and clearly showed fine spherical-shaped nanoparticles with several hundred nanometre diameter FONs (Fig. 5e). Similar sample preparation was also used to check the FON formation behaviour of the protonated ADA in acidic solution. As we expected, the orange and yellow fluorescent bright spots were observed in the preparation from acid THF/H_3O^+ mixing solutions at pH ~ 5.0 and ~4.0 as shown in Fig. 5b and c, respectively. Fig. 5d shows the interesting result that the green patterns in the image were observed in pure acidic aqueous solution (pH ~ 3.0), in accordance with the result of Fig. 2. Herein, fluorescence image-related TEM diagrams are presented in Fig. 5f–h. Combined with the experimental results of Fig. S10† and Fig. 5, ADA soluble in organic media is emissive (EA, THF and toluene, as shown in Fig. 1b). Moreover, the emission was not apparently enhanced in H_2O containing solution. Therefore, ADA should not be used as an AIE dye but rather as a "non-resonant exciton system" causing fluorescent aggregation. Usually, such dyes are emissive in organic solvents as well as in the solid state, even though they have a pi-stacking pattern. This result provides evidence that ADA possesses the potential of emissive-aggregates to form FONs regardless of neutral (ADA) or acidic conditions (ADA-H), which is helpful to infer information from the unique cellular images of ADA.

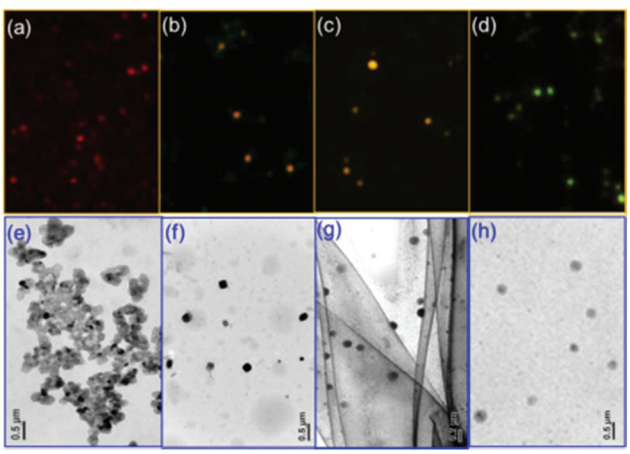

Fig. 5 FON illustrations for 50 μM of compound ADA. The fluorescence microscopy images that were prepared from (a) THF solution (cube: ex, 470/20 nm, 515 nm long pass filter); (b) THF/H_2O (v/v 1/3, pH ~ 5); (c) THF/H_2O (v/v 1/3, pH ~ 4) and (d) H_2O (pH ~ 3) (cube: ex, 390/10 nm bp filter; em, 410 nm lp filter). The relative TEM images are also shown in (e)–(h).

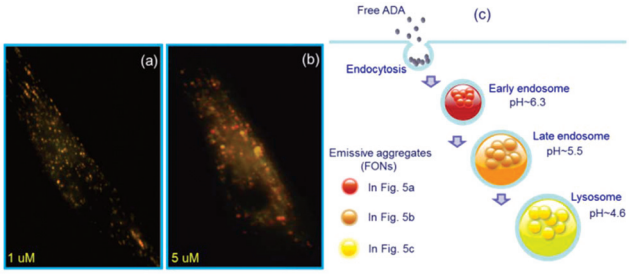

Fig. 6 Fluorescence images of MRC-5 normal cells stained with ADA 1 μM (a) and 5 μM for 4 hours (cube: ex, 390/10 nm bp filter; em, 410 nm lp filter). (c) pH-Dependent fluorescence mapping of the intracellular endocytosis pathway by ADA.

Concentration-dependent fluorescence cellular images further supported this model (Fig. 6). At low concentrations of ADA, intracellular fluorescent spots were homogeneous and dispersible. When higher concentrations of ADA were incubated, brighter speckles combined and dense spots were revealed in the images because the endocytosis pathway "enclosed" more molecules at a time. The compound ADA was characterized to present ICT response emission changes as well as aggregate-caused FONs against pH variation in spectral studies, which caused the intracellular endocytosis pathway-related colourful fluorescence spots regardless of whether the molecule was self-assembled or was enclosed by endocytosis. The summary is illustrated in Fig. 6c.

Conclusions

We designed and synthesized a pH sensor, ADA, whose emission response against the pH value was located in a range of cellular endocytosis pathways. From the results and discussions following the experiments, we initially identified that ADA penetrated cellular membranes through endocytosis and then changed their luminous properties by detecting different concentrations of protons within the endocytic vesicles. The pH fluctuation related to multi-colour emission changes within the endocytic pathways arose from the unique PET/ICT and the properties of emissive aggregates of ADA and is suitable for labelling intracellular pH dependent microenvironments.

Experimental

Materials

General chemicals employed in this study were of the highest grade available and were obtained from Merck Ltd or Acros/Aldrich Chemical Co. and used without further purification. All solvents for spectral measurements were of spectrometric grade.

Apparatus

Absorption and fluorescence spectra were recorded using a Thermo Genesys 6 UV–vis spectrophotometer and a HORIBA Jobin–Yvon Fluoromas-4 spectrofluorometer, respectively. Transmission electron microscopy (TEM) was conducted on a Zeiss EM 902A instrument operated at 80 kV. A mixed solution of THF and deionized water containing compound ADA was deposited onto a carbon-coated copper grid.

Determination of quantum yields

The quantum yields of NIM derivatives were determined as previously described using the following equation:[27]

$$\Phi_u = \Phi s \times [A_{fu} \times A_s(\lambda_{exs}) \times \eta_u{}^2]/[A_{fs} \times A_u(\lambda_{exu}) \times \eta_s{}^2]$$

where Φ_u is the quantum yield of the unknown; A_f is the integrated area under the corrected emission spectra; $A(\lambda_{ex})$ is the absorbance area at the excitation wavelength; η is the refractive index of the solution; the subscripts u and s refer to the unknown and the standard, respectively. For the same λ_{ex}, we chose 3, 6-bis (1-methyl-4-vinylpyridinium) carbazole diiodide (BMVC) as the standard, which has a quantum yield of 0.25 in glycerol and 0.02 in DMSO.[24,28]

Spectral response of ADA in pH variable solution

ADA was dissolved in DMSO to prepare a stock solution (10^{-2} M). The stock solution was diluted with water or DMSO to a concentration of 30 μM. Titration of ADA in DMSO: the acidic ADA/DMSO solution is achieved by adding very small amounts of 1M–0.1 M HCl solutions (volume <1%) to the 30 μM, 2 mL of ADA DMSO solution. At the same time, the control titration was also performed by adding an equal concentration of HCl (equal volume) to aqueous solution to calculate the pH at regular intervals. Each of these pH values were recorded and analysed by UV absorption and fluorescence emission. Excitation was at 450 nm or 400 nm; the emission range was from 420 to 750 nm.

Cell culture conditions and cellular imaging

MRC-5 human normal embryonic lung fibroblast cells and HeLa human cervical cancer cells were maintained in modified Eagle's medium (MEM) containing nonessential amino acids, Earle's salts, L-glutamine, 1 mM sodium bicarbonate, 1 mM sodium pyruvate, 1% penicillin/streptomycin, and 10% FBS. The CL1-0 human lung adenocarcinoma cancer cell line was grown in RPMI 1640 (Gibco/Invitrogen, Cat. no. 22400-089) medium containing 10% foetal bovine serum (FBS). The cells were cultured at 37 °C under a humidified atmosphere (95% air and 5% CO_2) and were then seeded onto coverslips and incubated for 24 h before observation by cellular imaging. On the next day, the cells were incubated with 5 μM of compounds for 4 h; here the DMSO stock solutions of the compounds were diluted in serum-free medium before use (1 : 100 v/v). The fluorescence images were taken under a Leica AF6000 fluorescence microscope with a DFC310 FX digital colour camera. The excitation sources were 390/10 nm or 470/20 nm bandpass for compounds. Fluorescence photographs were taken through related range tubes.

Intracellular pH calibration

In brief, cells were incubated with the compound for 4 h. The cover slips were rinsed 2 times with PBS buffer to remove the excess compound and then treated with PBS buffer at various pH values (3–7) in the presence of 5 μM of nigericin. After 5 min of incubation, nigericin was removed by gently rinsing with PBS (pH 7.4) twice, and then, PBS buffer solutions with varying pH values (3–7) were added to each cell line and incubated for 1 h at 37 °C. After that, the cells were rinsed twice again with neutral PBS buffer and transferred to the stage of the fluorescence microscope.

Cellular tracker assay

LysoTracker red assay: Cells were seeded onto chamber slides and incubated with ADA (5 μM) for 4 h at 37 °C. After that, the cells were gently washed with PBS twice and then incubated with fresh medium containing 30 nM Hoechst 33342 (ThermoFisher Scientific, Cat. no. H3570) and 100 nM LysoTracker red DND-99 (ThermoFisher Scientific, Cat. no. L7528) for 30 min at 37 °C. The fluorescent cellular images were finally obtained after washing with PBS twice. Rhodamine DHPE assay: cells were first incubated with ADA (6 μM) for 1 h at 37 °C. After that, the cells were gently washed with PBS twice and then incubated with fresh medium containing 30 nM Hoechst 33342 and 6 μM rhodamine DHPE (ThermoFisher Scientific, Cat. no. L1392) for 3 h at 37 °C. Cellular images were finally obtained after washing with PBS twice.

Synthesis

Details of the synthesis of NIM-1,[24] ABN[29] and ADA are described in the previous results and ESI† as shown in Scheme 1.

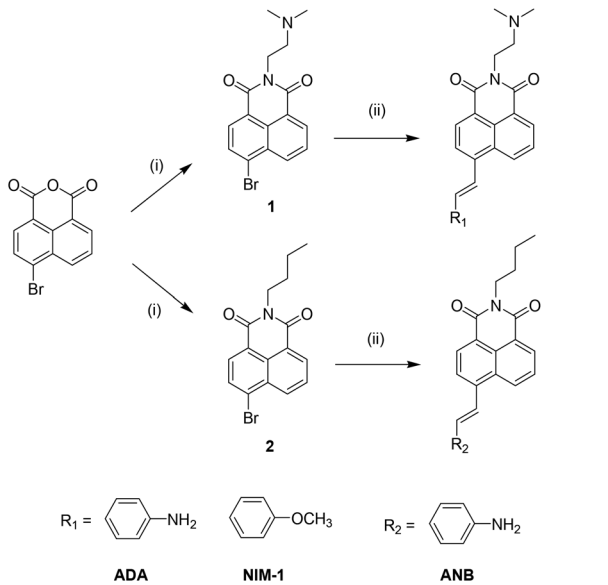

Scheme 1 Reagents and conditions: (i) *N*,*N*-Dimethylethane-1,2-diamine (ADA, NIM-1) or *n*-butylamine (ANB), EtOH, r.t. 24 h; (ii) $Pd(OAc)_2/(o\text{-}tol)_3P$, 4-vinylaniline (ADA, ANB), 4-methoxystyrene (NIM-1), Et_3N/MeCN, N_2, reflux, 48 h.

Conflicts of interest

There are no conflicts to declare.

Acknowledgements

This work was supported financially by the Ministry of Science and Technology, (MOST 104-2119-M-005-007-MY3) of Taiwan.

Notes and references

1 J. R. Casey, S. Grinstein and J. Orlowski, *Nat. Rev. Mol. Cell Biol.*, 2010, **11**, 50–61.
2 F. A. Gallagher, M. I. Kettunen, S. E. Day, D. E. Hu, J. H. Ardenkjær-Larsen, R. i. Zandt, P. R. Jensen, M. Karlsson, K. Golman, M. H. Lerche and K. M. Brindle, *Nature*, 2008, **453**, 940–943; Y. Kato, S. Ozawa, C. Miyamoto, Y. Maehata, A. Suzuki, T. Maeda and Y. Baba, *Cancer Cell Int.*, 2013, **13**, 89–96.
3 B. A. Webb, M. Chimenti, M. P. Jacobson and D. L. Barber, *Nat. Rev. Cancer*, 2011, **9**, 671–677.
4 P. Swietach, A. Hulikova, S. Patiar, R. D. Vaughan-Jones and A. L. Harris, *PLoS One*, 2012, **7**, e35949.
5 S. Mayor and R. E. Pagano, *Nat. Rev. Mol. Cell Biol.*, 2007, **8**, 603–612; I. Canton and G. Battaglia, *Chem. Soc. Rev.*, 2012, **41**, 2718–2739.
6 H. Lee, W. Akers, K. Bhushan, S. Bloch, G. Sudlow, R. Tang and S. Achilefu, *Bioconjugate Chem.*, 2011, **22**, 777–784; Y. Urano, D. Asanuma, Y. Hama, Y. Koyama, T. Barrett, M. Kamiya, T. Nagano, T. Watanabe, A. Hasegawa, P. L. Choyke and H. Kobayashi, *Nat. Med.*, 2009, **15**, 104–109; M. Grossi, M. Morgunova, S. Cheung, D. Scholz, E. Conroy, M. Terrile, A. Panarella, J. C. Simpson, W. M. Gallagher and D. F. O'Shea, *Nat. Commun.*, 2016, **7**, 10855–10868.
7 X. Ma, J. Cheng, J. Liu, X. Zhou and H. Xiang, *New J. Chem.*, 2015, **39**, 492–500; J. Han and K. Burgess, *Chem. Rev.*, 2010, **110**, 2709–2728; R. Wang, C. Yu, F. Yu, L. Chen and Y. Chunwei, *Trends Anal. Chem.*, 2010, **29**, 1004–1013.
8 Y. Feng, J. Cheng, L. Zhou, X. Zhou and H. Xiang, *Analyst*, 2012, **137**, 4885–4901.
9 Y. Hong, J. W. Y. Lam and B. Z. Tang, *Chem. Soc. Rev.*, 2011, **40**, 5361–5388.
10 B. K. An, J. Gierschner and S. Y. Park, *Acc. Chem. Res.*, 2012, **45**, 544–554.
11 H. Moon, Q. P. Xuan, D. Kim, Y. Kim, J. W. Park, C. H. Lee, H. J. Kim, A. Kawamata, S. Y. Park and K. H. Ahn, *Cryst. Growth Des.*, 2014, **14**, 6613–6619.
12 Z. Zhao, J. W. Y. Lam and B. Z. Tang, *J. Mater. Chem.*, 2012, **22**, 23726–23740; U. Rösch, S. Yao, R. Wortmann and F. Würthner, *Angew. Chem., Int. Ed.*, 2006, **45**, 7026–7030.
13 B. K. An, S. K. Kwon, S. D. Jung and S. Y. Park, *J. Am. Chem. Soc.*, 2002, **124**, 14410–14415; B. K. An, S. H. Gihm, J. W. Chung, C. R. Park, S. K. Kwon and S. Y. Park, *J. Am. Chem. Soc.*, 2009, **131**, 3950–3957; C. K. Lim, S. Kim, I. C. Kwon, C. H. Ahn and S. Y. Park, *Chem. Mater.*, 2009, **21**, 5819–5825; S. J. Yoon and S. Y. Park, *J. Mater. Chem.*, 2011, **21**, 8338–8346.
14 J. Gierschner and S. Y. Park, *J. Mater. Chem. C*, 2013, **1**, 5818–5832; F. Würthner, T. E. Kaiser and C. R. Saha-Möller, *Angew. Chem., Int. Ed.*, 2011, **50**, 3376–3410; C. S. Frank, *Acc. Chem. Res.*, 2010, **43**, 429–439; F. C. Spano, *Annu. Rev. Phys. Chem.*, 2006, **57**, 217–243; M. Kasha, H. R. Rawls and M. A. El-Bayoumi, *Pure Appl. Chem.*, 1965, **11**, 371–392.
15 K.-H. W. Joseph, H. T. Matthew and J. R. Peter, *Molecules*, 2017, **22**, 200–227; W. Yang, C. Li, M. Zhang, W. Zhou, R. Xue, H. Liu and Y. Li, *Phys. Chem. Chem. Phys.*, 2016, **18**, 28052–28060; J. Mei, N. L. Leung, R. T. Kwok, J. W. Lam and B. Z. Tang, *Chem. Rev.*, 2015, **115**, 11718–11940; R. T. Kwok, C. W. Leung, J. W. Lam and B. Z. Tang, *Chem. Soc. Rev.*, 2015, **44**, 4228–4238; J. Liang, B. Z. Tang and B. Liu, *Chem. Soc. Rev.*, 2015, **44**, 2798–2811.
16 Q. Feng, Y. Li, L. Wang, C. Li, J. Wang, Y. Liu, K. Li and H. Hou, *Chem. Commun.*, 2016, **52**, 3123–3126; Z. Yang, W. Qin, J. W. Y. Lam, S. Chen, H. H. Y. Sung, I. D. Williams and B. Z. Tang, *Chem. Sci.*, 2013, **4**, 3725–3730; J. Tong, Y. Wang, J. Mei, J. Wang, A. Qin, J. Z. Sun and B. Z. Tang, *Chemistry*, 2014, **20**, 4661–4670; D. Wu, L. Shao, Y. Li, Q. Hu, F. Huang, G. Yu and G. Tang, *Chem. Commun.*, 2016, **52**, 541–544; Z. Zhou, F. Gu, L. Peng, Y. Hu and Q. Wang, *Chem. Commun.*, 2015, **51**, 12060–12063.
17 C. G. Niu, G. M. Zeng, L. X. Chen, G. L. Shena and R. Q. Yu, *Analyst*, 2004, **129**, 20–24; D. Cui, X. Qian, F. Liu and R. Zhang, *Org. Lett.*, 2004, **16**, 2757–2760; S. Trupp, P. Hoffmann, T. Henkel and G. J. Mohr, *Org. Biomol. Chem.*, 2008, **6**, 4319–4322; A. P. de Silva, H. Q. N. Gunaratne, J. L. Habib-Jiwan, C. P. McCoy, T. E. Rice and J. P. Soumillion, *Angew. Chem., Int. Ed.*, 1995, **34**, 1728–1731; A. P. de Silva and T. E. Rice, *Chem. Commun.*, 1999, 163–164.
18 H. M. Kim, M. J. An, J. H. Hong, B. H. Jeong, O. Kwon, J. Y. Hyon, S. C. Hong, K. J. Lee and B. R. Cho, *Angew. Chem., Int. Ed.*, 2008, **47**, 2231–2234; X. Jin, J. Zhao, L. Zhang, Y. Huang and S. Zhao, *RSC Adv.*, 2014, **4**, 6850–6853.
19 R. Parkesh, L. T. Clive and T. Gunnlaugsson, *Org. Biomol. Chem.*, 2007, **5**, 310–317.
20 J. S. Yang, C. M. Wang, C. Y. Hwang, K. L. Liau and S. Y. Chiou, *Photochem. Photobiol. Sci.*, 2003, **2**, 1225–1231; F. Yu, Y. Wang, W. Zhu, Y. Huang, M. Yang, H. Ai and Z. Lu, *RSC Adv.*, 2014, **4**, 36849–36853; Z. R. Grabowski, K. Rotkiewicz and W. Rettig, *Chem. Rev.*, 2003, **103**, 3899–4032.
21 P. M. Haggie and A. S. Verkman, *J. Biol. Chem.*, 2007, **282**, 31422–31428.
22 M. Tafani, J. A. Cohn, N. O. Karpinich, R. J. Rothman, M. A. Russo and J. L. Farber, *J. Biol. Chem.*, 2002, **277**, 49569–49576.
23 L. A. Bagatolli and E. Gratton, *Biophys. J.*, 2000, **79**, 434–447.

24 H. H. Lin, Y. C. Chan, J. W. Chen and C. C. Chang, *J. Mater. Chem.*, 2011, **21**, 3170–3177.
25 S. Y. Su, H. H. Lin and C. C. Chang, *J. Mater. Chem.*, 2010, **20**, 8653–8658; H. H. Lin, S. Y. Su and C. C. Chang, *Org. Biomol. Chem.*, 2009, **7**, 2036–2039.
26 B. K. An, S. K. Kwon and S. Y. Park, *Angew. Chem., Int. Ed.*, 2007, **46**, 1978–1982.
27 L. F. V. Ferreiraa and S. M. B. Costab, *J. Lumin.*, 1991, **48–49**, 395–399.
28 C. C. Chang, S. H. Kuo, C. C. Kang and T. C. Chang, *J. Lumin.*, 2006, **119–120**, 84–90.
29 Y. T. Tung, C. C. Chang, Y. L. Lin, S. L. Hsieh and G. J. Wang, *Biosens. Bioelectron.*, 2016, **77**, 90–98.